J. Chem. Sci. Vol. 127, No. 4, April 2015, pp. 701–709. © Indian Academy of Sciences.
DOI 10.1007/s12039-015-0826-x

Studies on ethylbenzene dehydrogenation with CO_2 as soft oxidant over Co_3O_4/COK-12 catalysts

RAMUDU POCHAMONI[a], ANAND NARANI[a], MOHAN VARKOLU[a], MURALI DHAR GUDIMELLA[b], S SAI PRASAD POTHARAJU[a], DAVID RAJU BURRI[a], and SEETHA RAMA RAO KAMARAJU[a,*]

[a]Catalysis Laboratory, Indian Institute of Chemical Technology, Hyderabad, India
[b]Chemical Engineering Department, Gayatri Vidya Parishad College of Engineering, Visakhapatnam, India
e-mail: ksramarao@iict.res.in

MS received 17 July 2014; revised 28 October 2014; accepted 28 October 2014

Abstract. Oxidative dehydrogenation of ethylbenzene to styrene has been studied over Co_3O_4 supported on mesoporous silica (COK-12) with CO_2 as soft oxidant in a fixed bed reactor at atmospheric pressure in the temperature range of 723 to 923K. While COK-12 has been prepared by self-assembly method using long chain ionic surfactant i.e., P123 as template, cobalt oxide supported on COK-12 catalysts with variable Co content have been synthesised by simple wet impregnation technique. All the catalysts were characterized by N_2 adsorption - desorption, XRD, FT-IR, TPR, UV-Vis and XPS techniques. XRD and pore size distribution studies indicate the intactness of mesoporous structure of SiO_2 even after incorporation of Co_3O_4. Presence of Co_3O_4 crystallites were observed beyond 5 wt% Co loading. High ethylbenzene conversion and stable styrene yields have been observed over 3% Co_3O_4/COK-12 catalyst due to the presence of large number of active Co_3O_4 catalytic sites. Enhancement in the activity has been observed with CO_2 as soft oxidant than with N_2 as diluent. This is because of the fact that the liberated H_2 reacts with CO_2 in the form of reverse water gas shift reaction.

Keywords. Co_3O_4/COK-12; ethylbenzene; dehydrogenation; CO_2; soft oxidant; styrene.

1. Introduction

Styrene is one of the most important monomer which is widely used as a feedstock for production of styrene polymers such as polystyrene (PS), acrylonitrilebutadiene-styrene (ABS), styrene-acrylonitrile (SAN), in addition topolyolefins and poly (vinyl chloride), an important group of thermoplastics.[1] The production of over 90% of styrene in the world is based on the catalytic dehydrogenation of ethylbenzene.[2] However dehydrogenation of ethylbenzene process is extremely endothermic reaction. In the industrial process of ethylbenzene dehydrogenation, steam at high temperatures (873 to 973K) is being introduced to produce styrene.[2–5] Pumping of steam along with ethylbenzene is helpful to some extent in removing the coke formed on the surface of the catalyst. However, the major challenge associated with the dehydrogenation of ethylbenzene is the development of selective and stable catalyst which has to with stand the high reaction temperature and resistant to coking.

Oxidative dehydrogenation (ODH) process gains importance in recent times mainly due to the shifting of equilibrium to the product side.[2] Generally, the oxidants employed in ODH process are oxygen, sulphur dioxide, dry air, dinitrogen oxide and carbon dioxide.[6–9] Though the process becomes exothermic with O_2 as oxidant, sometimes it is difficult to control overoxidation. In this connection, CO_2 has been recognised as one of the effective soft oxidants for the oxidative dehydrogenation of ethylbenzene. In the oxidative dehydrogenation of ethylbenenzene, $CO_2$is converted into CO via reverse water gas shift reaction (RWGSR).[10] In other words, CO_2 can be used in the form of reverse water-gas shift reaction coupled with dehydrogenation reactions.[2] The overall dehydrogenation of ethylbenzene in the presence of steam is an endothermic reaction. The catalytic dehydrogenation of ethylbenzene with oxygen is an exothermic reaction. Though the catalytic dehydrogenation of ethylbenzene in the presence of CO_2 is endothermic reaction it offers several advantages compared to the reaction with steam as diluent. Apart from the ecological point of view, the main advantage associated with CO_2 as soft oxidant is higher equilibrium conversion of ethylbenzene than with steam.

In the past decades, many research groups used CO_2 as a soft oxidant in ODH over transition metal

*For correspondence

oxides, such as iron oxide, vanadium oxide, TiO_2–ZrO_2 mixed oxide, hydrotalcite-like oxide, spinel oxide and Fe-containing ceramic composites.[11–28] Different supporting cobalt catalysts have been investigated for dehydrogenation of ethylbenzene, such as iron oxide, aluminium pillared clay, carbon nanotube MCM-41 and hydrotalcites.[5,9,29–33] Among these, the catalysts containing mesoporous molecular sieves as supports have shown good results due to the presence of high surface area and ordered structure.[8] Recently, mesoporous molecular sieve-supported oxide materials such as SBA-15, MCM-41, and silicalitemesoporous zeolite have been investigated as catalysts and supports. The advantages of these materials are that they have high thermal stability and possess very high surface area with a uniform pore-size distribution which allow better dispersion of active component and thereby results in the enhancement of catalytic activity. These are found to be the most promising materials for the dehydrogenation of ethylbenzene in the presence of CO_2 as soft oxidant.[8,34–37]

Herein, we report for the first time COK-12 (hexagonal mesostructured silica) supported cobalt oxide catalysts for the oxidative dehydrogenation of ethylbenzene by using CO_2 as soft oxidant.

2. Experimental

2.1 *Catalyst preparation*

Generally, hexagonally ordered mesoporous material is obtained by heating. In the synthesis protocol, particularly for the synthesis of SBA-15, MCM-41, heating was necessary.[38,39] But Jammaer *et al.*, reported a new method for synthesis ordered mesoporous silica (COK-12) material with large pore sizes obtained even at room temperature and without stirring.[40] It typically leads to larger pore size and larger mean pore diameter (6.9 nm) than SBA-15 (5.7 nm). Herein, for the preparation of COK-12, self-assembly method using long chain ionic surfactant i.e., P123(M/s. Sigma Aldrich Chemicals, USA) as template and sodium silicate as SiO_2 source as reported by Jammaer *et al.*, has been adopted.[40] Briefly, COK-12 was prepared by dissolving 4.0 g of the triblock co-polymer Pluronic, P123 in 107.5 g water. To this solution, 3.684g citric acid monohydrate (M/s. SD Fine Chem. Ltd., India) and 2.540g trisodium citrate (M/s.SD Fine Chem. Ltd., India) were added. The resulting solution was stirred for 24 h. 10.4 g sodium silicate solution (10% NaOH, 27% SiO_2, M/s. Merck, Germany) in 30.0 g of H_2O was added to the solution containing P123, citric acid and sodium precursor. The solution was stirred for 5 min at 175 rpm and kept at room temperature without agitation for 24 h. The as-synthesized material was filtered, washed and dried at 333K overnight. Finally the material was calcined in air in two steps, 8 h at 573K followed by 8 h at 773K with 1K min^{-1} ramp. All cobalt metal oxides supported on COK-12 catalysts were prepared by wet impregnation technique. $Co(NO_3)_2.6H_2O$ was used as a Co precursor. All the catalysts were calcined in air at 723K at 5 h with ramping 10 K m^{-1}. The catalysts were designated as xCC12 where 'x' stands for Co_3O_4 loading in weight percent.

2.2 *Catalyst characterization*

XRD patterns of the catalysts were recorded on a Rigaku Ultima−IV (M/s. Rigaku Corporation, Japan) X−ray diffractometer with Ni filtered Cu Kα radiation ($\lambda = 1.5406$ Å) with a scan speed of 4° min^{-1} and a scan range of 2–80° at 40 kV and 20 mA. In order to confirm the mesoporous nature of the COK-12, low angle XRD patterns were obtained in a scan range of 0.7−5°.

The FT−IR patterns were recorded on a spectrum GX spectrometer (M/s. Perkin-Elmer, Germany) in the scan range of 4000–400 cm^{-1}.

Temperature programmed reduction (TPR) was performed in a laboratory-built equipment containing a quartz reactor with electrical heating and a thermal conductivity detector (TCD) equipped gas chromatograph. About 100 mg of catalyst placed at the centre of the quartz reactor between two plugs of quartz wool was pre-treated at 573K for 1 h in Ar flow (60 cm^3 min^{-1}). Then the catalyst was exposed to 5% H_2 balance Ar gas flow for 1 h at 373K followed by raising the temperature of sample up to 1073K at a heating rate of 10K min^{-1}. The H_2 gas consumption was monitored with standard GC software.

Brunauer, Emmett and Teller (BET) equation is used to calculate the surface area whereas Barret-Joyner-Halenda (BJH) method is used to obtain the pore size distribution of the catalysts. For this purpose, N_2 adsorption-desorption experiments were conducted at 77K on an Autosorb Instrument (M/s. Quantachrome, USA). Prior to N_2 adsorption-desorption experiment, the catalyst was degassed under vacuum at 573 K for 3 h to remove the physisorbed moisture.

The morphological features of the catalysts were obtained using a JEOLJEM 2000EXII transmission electron microscope, operating between 160 and 180 kV. The specimens were prepared by dispersing the powder samples in methanol using an ultrasonic bath and evaporating a drop of resultant suspension onto the lacey carbon support grid.

The UV–vis diffused reflectance spectra were recorded on Perkin Elmer UV WinLab spectrometer with an integrating sphere reflectance accessory. The spectra were recorded in UV–vis region of 200–800 nm.

2.3 *Catalysts tests and analytic procedure*

Dehydrogenation of ethylbenzene was carried out in a continuous down flow fixed bed reactor operated at atmospheric pressure. In each catalytic run, about 1g of catalyst diluted with an equal amount of silica beads, was positioned between two layers of quartz wool at the centre of the reactor. The upper portion of the reactor was filled with silica beads that served both as a pre-heater and a mixer for the reactants. Prior to reaction, the catalyst was exposed to N_2 gas ($20cm^3min^{-1}$) at 873K for 1h. After bringing the reactor temperature to the required temperature, ethyl benzene was fed ($1cm^3h^{-1}$) into the reactor through a microprocessor controlled metering pump (M/s. B.Braun, Germany). Along with ethylbenzene, N_2 or CO_2 flow (20 cm^3 min^{-1}) was maintained. The reaction was carried out in a temperature of 723 to 923K. The liquid product mixture was collected in a trap kept at $-10°C$ at hourly intervals. The products were analyzed by a Flame Ionization Detector (FID) equipped gas chromatograph, GC - 17A (M/s. Shimadzu Instruments, Japan) with OV-1 capillary column (30 m length, 0.53 mm id) and the components were confirmed by GC−MS. (Model: QP 5050, M/s. Shimadzu Instruments, Japan). Ethylbenzene conversion has been calculated as following equations:

$$\text{EB Conversion} = \left(\frac{EB_{in} - EB_{out}}{EB_{in}}\right) \times 100 \quad (1)$$

$$\text{STY selectivity} = \left(\frac{STY_{out}}{Products_{out}}\right) \times 100 \quad (2)$$

3. Results and Discussion

Figure 1 shows the XRD patterns of COK-12 and supported cobalt oxide catalysts. The inset of figure 1 is the low angle XRD patterns and the wide angle patterns are shown in figure 1. Low angle XRD patterns of both pure COK-12 and all catalysts indicate three well-resolved diffraction peaks at 2θ values between 0.7° and 5°. These peaks can be indexed as the (100), (110) and (200) peaks, which indicates the presence of highly ordered hexagonal mesoporous structure, p6m.[40] The presence of additional (210) and (300) higher order reflections revealed the high quality of the ordering.[40] In the present case, compared to the (100) reflection, other characteristic reflections of the mesoporous silica, (110) and (200) reflections, are not clearly visible from the small-angle XRD patterns. This is an indication that the synthesized mesoporous silica COK-12 was less ordered than that reported in the literature.[41,42] It is noteworthy that COK-12 still exhibits a high degree of mesoporous structure even at the highest cobalt loading. However, all the catalysts exhibit a significant reduction of the (100) peak intensity relative to COK-12. As the cobalt content increases the intensity of the (100) peak decreases. This can be explained by the presence of cobalt oxide nanoparticles inside mesoporous channels of COK-12.[43,44] Pour filling in turn, reduces scattering contrast between the pores and the walls of the support.[45]

Figure 1 shows the wide-angle XRD patterns of all catalysts with different cobalt content. As expected, COK-12 does not show any sharp diffraction peaks consistent with the amorphous structure of the support. However, a broad peak at $15° < 2\theta < 30°$ is observed in the diffraction patterns of COK-12 and all catalysts corresponding to the amorphous silica phase.[46] XRD patterns of the catalysts with lower Co_3O_4 loadings, do not display any diffraction pattern attributed to cobalt oxide. This can be attributed to the low cobalt content and high dispersion of the cobalt oxide species on the support.[47] However, XRD patterns of the catalysts with higher Co_3O_4 loadings show diffraction peaks corresponding to Co_3O_4 spinel(JCPDS No. 00-042-1467). The diffraction peaks at $2\theta = 18.8°$, 31.1°, 36.7°, 38.2°, 44.6°, 59.2°, 65.1° and 77° confirmed the crystallized spinel Co_3O_4 with space group *Fd3m*.[48]

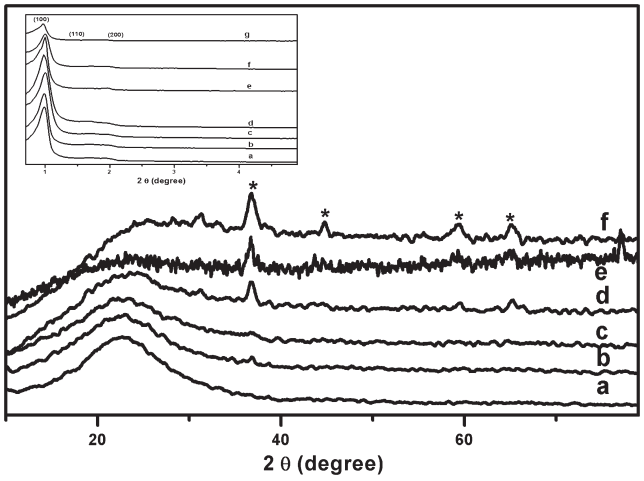

Figure 1. (Inset) Low angle XRD patterns of Co_xO_y/COK-12 catalysts: a) C12, b) 1CC12, c) 3CC12, d) 5CC12, e) 8CC12, f) 10CC12 and g) 12CC12. Wide angle XRD patterns of Co_xO_y/COK-12 catalysts: a) 1CC12, b) 3CC12, c) 5CC12, d) 8CC12, e) 10CC12, and f) 12CC12.

The average Co_3O_4 particle size was calculated from the full-width at half-maximum of the most intense peak of the Co_3O_4 diffraction signal by using Debye-Scherrer equation (Equation 3):

$$d = \frac{0.89\lambda}{\beta \cos\theta} \quad (3)$$

Where d is the Co_3O_4 particle size, λ is the X-ray wave length (1.5406 Å), and β is the full width half maximum of Co_3O_4 diffraction peak. The average Co_3O_4 particle sizes of all the catalysts were displayed in table 1. The Co_3O_4 particle size in the catalyst with 8% Co_3O_4 content is 9 nm and that in 10 % Co_3O_4 content is 13 nm. For the catalyst with 12% Co_3O_4 content, the particle size increases sharply to 39 nm. No XRD signals due to Co_3O_4 crystallites are found in the XRD patterns of catalysts containing 3 and 5 weight % Co_3O_4 which clearly indicates that the crystallite size of Co_3O_4 is below the detection capacity of XRD i.e., below 4 nm.

The N_2 adsorption–desorption isotherms of COK-12 and various cobalt oxide loaded catalysts are displayed in figure 2. It can be seen that all samples display a type IV isotherm with an H1 hysteresis loop, characteristic of ordered mesoporous materials.[49] The N_2 adsorption isotherm of COK-12 shows a sharp inflection at a relative pressure in the range of 0.7–0.9 (figure 2) indicative of a good-quality COK-12 material with uniform mesopores and the isotherms of Co_3O_4/COK-12 samples are similar to that of the original COK-12, suggesting that the mesoporous structure of all supported catalysts are mostly retained upon cobalt deposition. The inflection of the adsorption branch of the isotherms occurred at a lower relative pressure (0.55–0.80) for cobalt oxide containing samples as compared to the pure support, indicating a decrease of the mean pore diameter after cobalt deposition. Both BET surface area and total pore volume have been significantly decreased upon cobalt oxide impregnation, and this tendency is greater at higher Co_3O_4 loadings. This may be due to the deposition of cobalt oxide particles on the surface of parent COK-12 and partial blockage of the support pores by cobalt oxide clusters and/or a partial collapse of the mesoporous structure. The BET surface area, pore volume, pore diameter and pore wall thickness are depicted in table 1. As shown in the PSD curve (inset of figure 2), the pores are distributed in the range of 5–13 nm. Hence, in the catalysts with lower Co_3O_4 loadings (3 &5%), there is a chance for the Co_3O_4 particles present inside the pores of COK-12.

Figure 3 shows the FT-IR spectra of COK-12 and the various loadings of cobalt oxide catalysts. The FT-IR spectrum of COK-12 consists of absorption bands at 1087, 807 and 464 cm^{-1}, which arise from the Si−O−Si stretching vibration. The absorption band

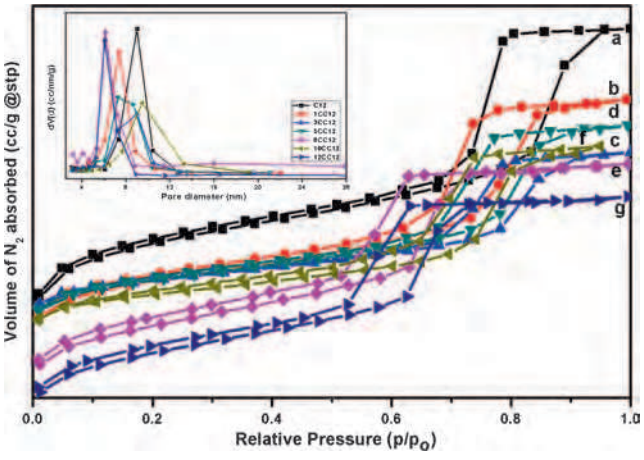

Figure 2. N_2 adsorption – desorption patterns of Co_xO_y/COK-12 catalysts: a) C12, b) 1CC12, c) 3CC12, d) 5CC12, e) 8CC12, f) 10CC12, g) 12CC12 (Inset: Pore size distributions graphs).

Table 1. Physico-chemical characterization of Co_3O_4/COK-12 catalysts.

Catalyst	S^a_{BET} (m^2/g)	V^b_t (cc/g)	D^c_{BJH} (nm)	d^d_{100} (nm)	a^e_0 (nm)	t^f (nm)	Cobalt oxide particle size (nm)
COK-12	488.720	0.58	4.758	9.0141	10.409	5.659	–
1CC12	278.759	0.41	6.003	8.8127	10.176	4.173	–
3CC12	229.861	0.35	6.082	8.9921	10.383	4.301	–
5CC12	192.059	0.29	6.113	8.9105	10.289	4.176	–
8CC12	220.473	0.37	5.471	8.8339	10.200	4.729	9.07
10CC12	193.005	0.32	6.720	8.8738	10.247	3.527	12.63
12CC12	213.423	0.36	5.68	8.9958	10.387	4.707	39.10

[a]BET surface area.
[b]The total pore volume.
[c]BJH average pore diameter.
[d]Periodicity derived from low angle XRD.
[e]The unit cell parameter ($a_0 = 2\ d100/\sqrt{3}$).
[f]The pore wall thickness($t = a_0 - D_{BJH}$).

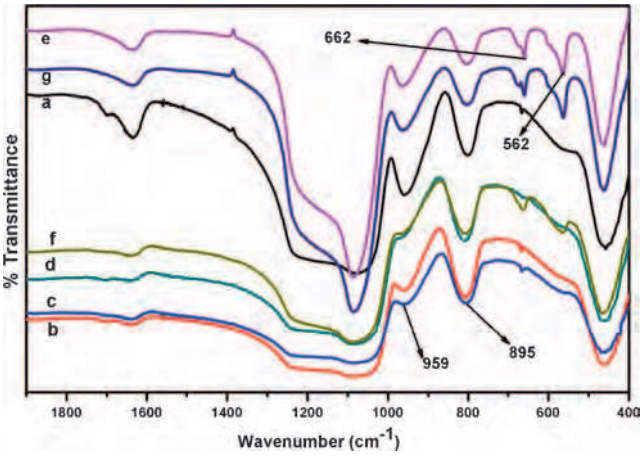

Figure 3. FT-IR spectra of Co_xO_y/COK-12 catalysts: a) 1CC12, b) 3CC12, c) 5CC12, d) 8CC12, e) 10CC12, f) 12CC12.

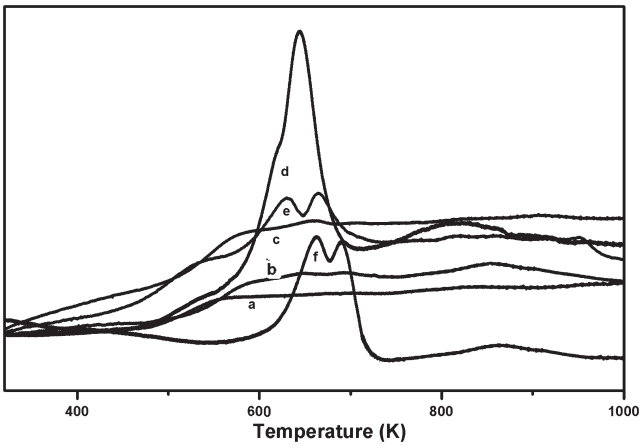

Figure 4. TPR patterns of Co_xO_y/COK-12 catalysts: a) 1CC12, b) 3CC12, c) 5CC12, d) 8CC12, e) 10CC12, f) 12CC12.

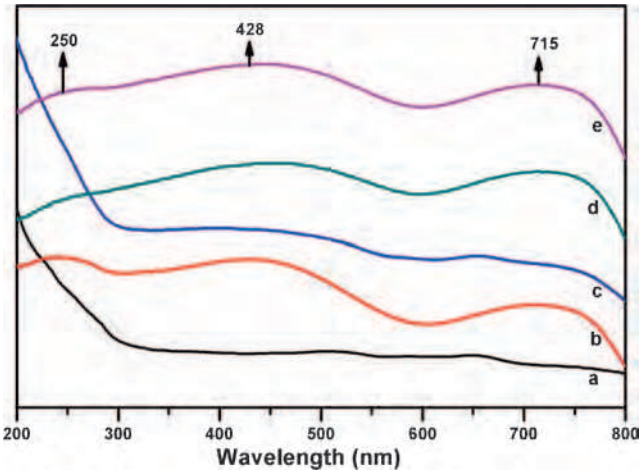

Figure 5. UV-vis spectra of Co_xO_y/COK-12 catalysts: a) 1CC12, b) 3CC12, c) 5CC12, d) 8CC12, e) 10CC12, f) 12CC12.

at around 960 cm^{-1} can be assigned to either Si−OH or Si−O−Si stretching vibrations. The broad band at around 3400 cm^{-1} is due to the presence of surface −OH groups with strong H-bonding interactions between them. Finally the band at around 1630 cm^{-1} can be assigned to the deformation modes of −OH bonds of adsorbed H_2O.[50] The FT-IR spectra of low Co_3O_4 loading catalysts exhibit a very similar spectrum to that of COK-12.Beyond 8 % Co_3O_4 content, the patterns exhibit two additional bands at around 662 and 562 cm^{-1} (black arrows). These latter bands can be ascribed to Co−O vibrations in the cobalt oxide lattice.[48] It indicates the formation of crystalline Co_3O_4 beyond 8 wt% of cobalt oxide which is supported by wide angle X-ray results (figure 1).

H_2-TPR profiles of COK-12 supported cobalt oxide with different loadings are shown in figure 4. According to the literature Co_3O_4 gets reduced in two stages; the low temperature one (∼493 K) is due to the reduction of Co_3O_4 to CoO and the high temperature signal (∼573 K) is due to the reduction of CoO to Co.[51,52] The reduction of bigger particles of Co_3O_4 species gets reduced at lower temperatures and the reduction of cobalt oxide species which are more interactive with silica surface gets reduced at high temperatures.[51] The TPR curves of the COK-12 supported samples show one broad peak at a T_{max} below 600 K, probable due to the reduction of Co_3O_4. Apparently the subsequent reduction signal due to the reduction of CoO to Co might have merged with the first signal. With increase in Co content, formation of bigger Co_3O_4 particles results which are expected to get reduced at lower temperatures. However, in the present case, the T_{max} shifts to higher temperatures as the Co content increases. This may be due to more extensive filling of COK-12 pores with Co_3O_4 at higher Co loadings. It is reported that the Co_3O_4 particles trapped inside the pores are difficult to reduce.[48] It is also reported that the cobalt oxide species which are present in the form of as Co-silicate like species gets reduced at higher temperatures i.e., beyond 873 K.[52–54] Thus the TPR pattern of 12CC12 catalyst indicates two high temperature maxima, one in the temperature range of 873–898 K due to the reduction of Co_3O_4 interacted species with SiO_2 or the bigger Co_3O_4 species trapped inside the pores. The other signal present in the temperature zone of 898–923 K is due to the reduction of Co-silicate like species.

Figure 5 displays the diffuse reflectance (DR) UV-vis spectra of Co_3O_4 catalysts. From the diffuse reflectance (DR) UV-vis technique, it is possible to find out the local environment of cobaltoxide in the mesostructure COK-12. Figure 5 displays three distinct absorption bands. The absorption band at around ∼250 nm can be assigned to the charge transfer from O^2 to Co^{+3}.[48]

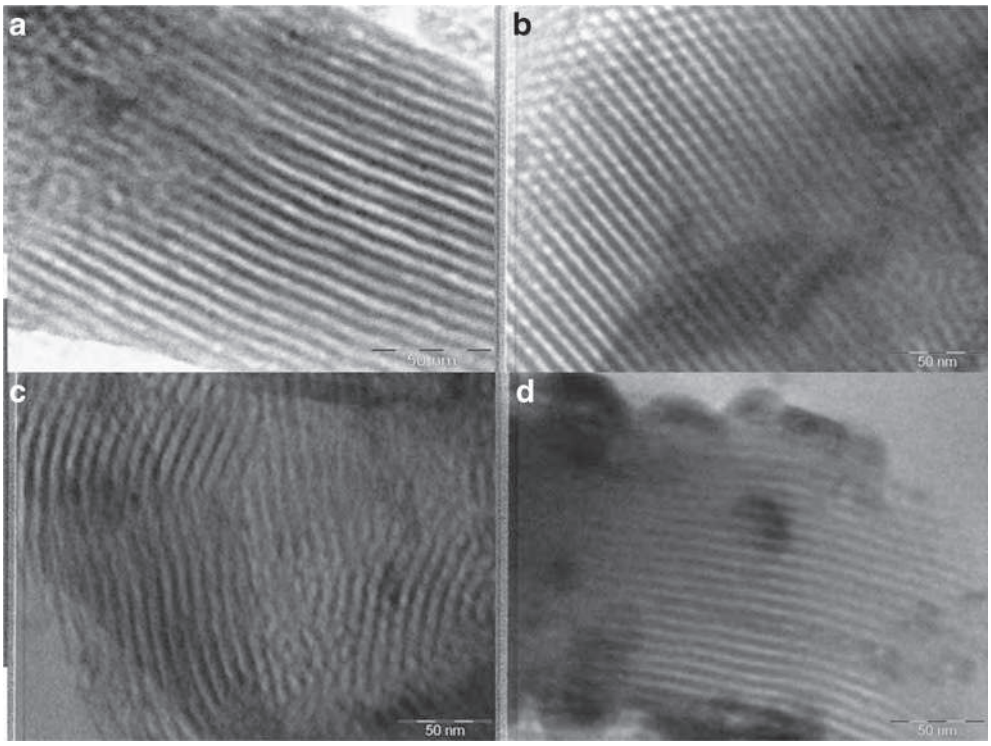

Figure 6. TEM images of Co_xO_y/COK-12 catalysts: a) C12, b) 1CC12, c) 3CC12, d) 12CC12.

The second absorption band at around 420 nm can be attributed to octahedrally coordinated Co^{+3} in well ordered spinal Co_3O_4 species and third absorption band at around 720 nm is ascribed to the electronic ligand field $^4A_2$ (F) $\rightarrow$ $^4T_1$ (p) transition of Co^{+2} in tetrahedral coordination.[48,55,56]

Figure 6 shows the TEM pictures of COK-12, 3%Co_3O_4/COK-12 and 12%Co_3O_4/COK-12 catalysts. In all the catalysts, it is clear that the mesoporous network is intact. It was reported that the typical hexagonal structures of COK-12 are well displayed for all prepared samples and are still maintained after Pd loading.[41] In our recent publication, it was shown from the TEM images that the well ordered hexagonal arrays of mesoporous network was maintained after deposition of MoO_3 on COK-12 support.[60] Both TEM and SAXS data provides a valuable information about the uniform pore structure. Even though the surfactant (P123) is same in the synthesis of COK-12 and SBA-15, there seem to be differences in the formation process.According to the findings of Stucky *et al.,* strong electrostatic interactions play a key role in the formation SBA-15 assembly.[61] On the other hand, in the synthesis of COK-12, no such electrostatic interactions exists.[44]

The dehydrogenation of ethylbenzene has been carried out in a fix bed reactor under atmospheric pressure with co-feeding of either inert gas (N_2) or CO_2 gas as soft oxidant over cobalt oxide supported COK-12

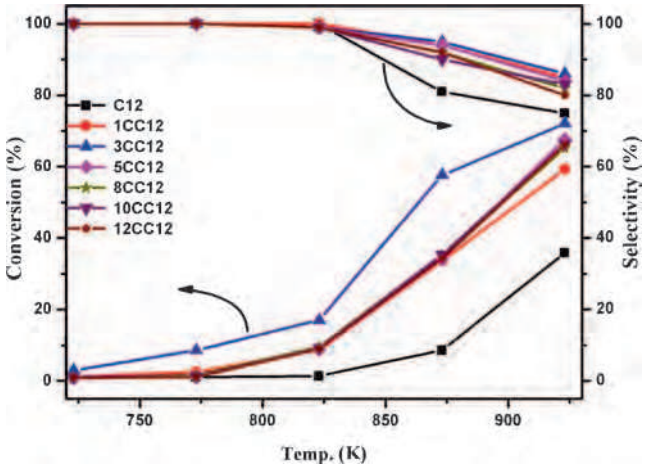

Figure 7. Effect of temperature on the activity under CO_2 flow over Co_xO_y/COK-12 catalysts: Reaction conditions: 1 atm, T=723K – 923K, 1g catalyst, EB flow= 1mL/h, N_2/CO_2 flow=20mL/min a) C12, b) 1CC12, c) 3CC12, d) 5CC12, e) 8CC12, f) 10CC12, g) 12CC12.

catalysts. There are no reports available for dehydrogenation of ethylbenzene over Co_3O_4/COK-12 catalysts, but some research groups are working on the Co catalysts with different supports for dehydrogenation of ethylbenzene.[33–39,57–59] Figure 7 and 8 show the catalytic activity of various loadings of cobalt oxide supported on COK-12 catalysts for dehydrogenation of ethylbenzene with CO_2 as soft oxidant and inert gas (N_2) flow respectively at various temperatures. Pure support, COK-12 and bulk Co_3O_4 exhibits poor

dehydrogenation activity for the conversion of ethylbenzene. Over Co_3O_4/COK-12 catalysts, the conversion increases with increase in cobalt oxide loading up to 3wt% and beyond this loading the ethyl benzene conversion decreasesboth in presence of CO_2 and N_2 flows. Catalysts with higher cobalt loadings show poor Co_3O_4 dispersion due to the formation of bigger Co_3O_4 species on surface of COK-12. Formation of bigger Co_3O_4 particles was clearly witnessed from the results of wide angle XRDFT-IR and TPR. Decrease in surface area with increasein cobalt oxide loading (table 1) is also due to the formation of bigger Co_3O_4 particles which block the pores of the support. The Co_3O_4 dispersion of 3CC12 as measured by CO pulse chemisorptions under dynamic conditions is 26% and this value decreases with increase in Co_3O_4 loading. Even though, the surface coverage of Co_3O_4 on the 3CC12 catalyst is only 2.5%, its activity in ethylbenzene dehydrogenation is very high. Compared with N_2 co-feeding (figure 8), CO_2co-feeding (figure 7) is advantageousin terms of yielding higher conversion of ethylbenzene and higher selectivity towards styrene. In both CO_2 and N_2co-feeding, the ethylbenzene conversion increases with increase in temperature. But, the selectivity towards styrene decreases with raise in temperature which might be due to coke formation on surface.[8] Mathew *et al.*, reported low conversions of ethylbenzene and low selectivity of styrene at 698 K on Cu, Co and Fe mixed oxide catalyst.[33] Guo *et al.* Reported 88% ethylbenzene conversion but with low styrene selectivity on higher loadings of cobalt on carbon nano tube catalysts at 823 K.[36]

As shown in figures 7 and 8, cobalt oxide supported on COK-12 catalysts show good catalytic activity towards ethylbenzene especially under CO_2 flow. Figure 9 shows the time on steam study at 873 K under N_2 and CO_2co-feedings separately over 3 wt % cobalt oxide catalyst. Initial ethylbenzene conversion of ~60% falls gradually and reaches to ~40% in 24 h time in N_2 flow and the styrene selectivity also follows the same trend (~80% in the 1st hour to ~50% at the end of 24 h). On the other hand, under soft oxidant, CO_2 flow, steady ethylbenzene conversion of ~55% and high selectivity towards styrene (95%) was maintained throughout the time on stream study. The presence of CO_2 as oxidant in the dehydrogenation reaction leads to selective product formation and minimizes the deactivation of the catalyst. The Co_3O_4 content (determined

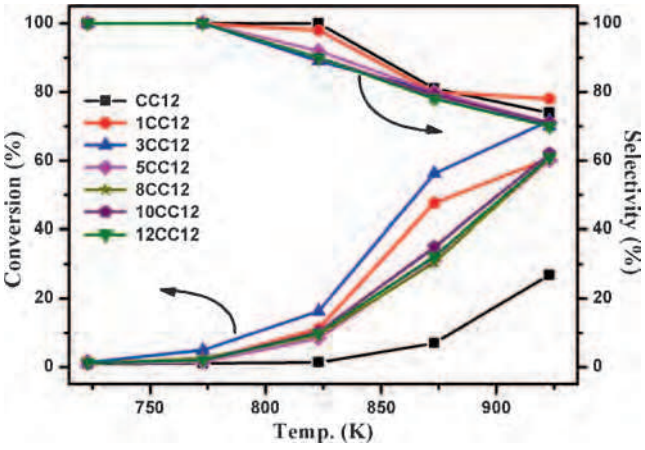

Figure 8. Effect of temperature on the activity under N_2 flow over Co_xO_y/COK-12: Reaction conditions: Same as for figure 7 a) C12, b) 1CC12, c) 3CC12, d) 5CC12, e) 8CC12, f) 10CC12, g) 12CC12

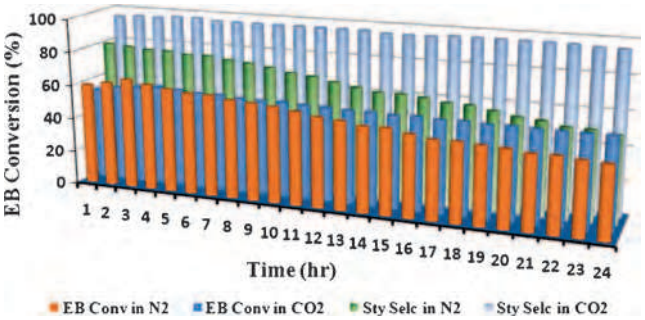

Figure 9. Time on stream studies under both CO_2 and N_2 flow over 3CC12: Reaction conditions: 1 atm, T=873K, 1g catalyst, EB flow= 1 mL/h, N_2/CO_2 flow=20mL/min.

Ethyl benzene → Styrene + H_2 (Ethyl benzene Dehydrogenation)

CO_2 + H_2→ CO + H_2O (RWGS)

EB + CO_2→ Styrene + CO + H_2O

Scheme 1. Ethylbenzene dehydrogenation in presence of CO_2.

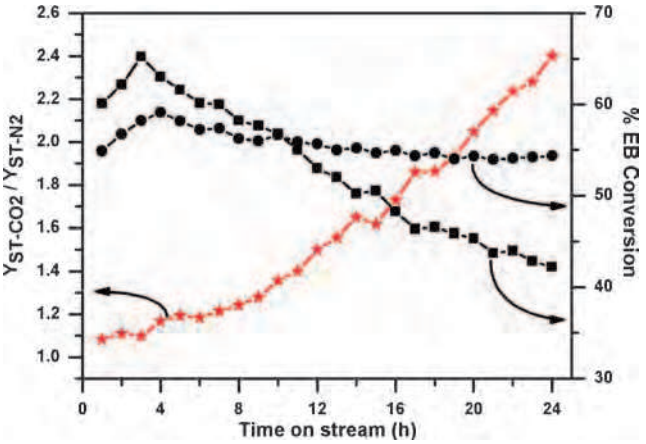

Figure 10. EB conversions and styrene yields ratio in the presence of CO_2 and N_2 atmospheres (Y_{ST-CO2}/Y_{STY-N2}) over 3CC12. Reaction conditions: Same as for figure 9.

Table 2. Comparison of EB dehydrogenation ability of 3% Co_3O_4/COK-12 with 14% MoO_3/COK-12 catalyst in N_2 and CO_2 flow at 873 K.

Catalyst	EB Conversion (%)		STY Selectivity (%)		Y_{ST-CO2}/Y_{STY-N2}	Reference
	In CO_2	In N_2	In CO_2	In N_2		
3 % Co_2O_3/COK-12	57.5	55.8	95.5	80	1.23	Present investigation
14% MoO_3/COK-12	57.2	75.3	71.4	47	1.15	[58]

by ICPMS) in the fresh catalyst (2.45 wt%) is same as that obtained in the spent catalyst in CO_2 flow (2.45 wt%). However, the Co_3O_4 content in the spent catalyst in N_2 flow is only 1.63 wt%. This is due to the formation of coke on the catalyst which was subjected to ethylbenzene along with N_2. Because of coking the catalyst suffers its activity in N_2 flow. On the other hand, in CO_2 flow, steady styrene selectivity over prolonged times was maintained. The role of CO_2 as soft oxidant is due to its participation in the form of reverse water-gas-shift (RWGS) reaction coupled with the simple ethyl benzene dehydrogenation (scheme 1).

The styrene yields in presence of CO_2 and N_2 (Y_{ST-CO2}/Y_{STY-N2}) indicate the beneficial role of CO_2 in the dehydrogenation of ethylbenzene. Figure 10 indicates the promotional effect of CO_2 particularly in yielding higher value of Y_{ST-CO2}/Y_{STY-N2}. CO_2 promotional effect can be seen from the rising of Y_{ST-CO2}/Y_{STY-N2} almost linearly from 1.08 in the first hour to 2.40 at the end of 24 h. Exhibition of higher styrene selectivity in CO_2 flow than in N_2 flow can also be seen over MoO_3/COK-12 catalysts reported in our earlier publication.[60] From this publication, the optimum loading of MoO_3 was found to be 14% by weight for getting good ethylbenzene conversion. Table 2 compares the ethylbenzene dehydrogenation ability of 3% Co_3O_4/COK-12 catalyst (present investigation) with that of 14% MoO_3/COK-12 catalyst, reported earlier.[60] Even though higher ethylbenzene conversion (∼75%) is observed in N_2 flow over 14% MoO_3/COK-12, the styrene selectivity is very low (47%). In CO_2 flow over this catalyst, the ethyl benzene conversion is ∼56%, but styrene selectivity is 80%. On the other hand, 3% Co_3O_4/COK-12 exhibits more or less same ethyl benzene conversion (55%) in both N_2 and CO_2 flows, but higher styrene selectivity is observed in CO_2 flow (∼96%) than in N_2 flow (71%).

4. Conclusions

The activity of Co_3O_4/COK-12 catalyst for the oxidative dehydrogenation of ethylbenzene in the presence of CO_2 revealed that mesoporous silica COK-12 material is the promising support for the development of highly active and selective catalyst. It can be concluded that low loading cobalt metal oxide supported on COK-12 (3 weight %) is sufficient to yield a good amount of styrene in the oxidative dehydrogenation of ethylbenzene in the presence of CO_2 which is not the case with MoO_3/COK-12 catalysts. At lower loading of cobalt oxide, it is in the highly dispersed form on COK-12 support. The soft oxidant CO_2 is the prominent promoter for the dehydrogenation of ethylbenzene compared with N_2. Time on stream studies reveal the steady maintenance of ethyl benzene conversion with high styrene selectivity over 3% Co_3O_4/COK-12 catalyst in presence of CO_2 rather than in N_2.

Acknowledgements

The authors thank Department of Science & Technology (DST), New Delhi, India for sanctioning a project (DST/IS-STAC/CO_2-SR-136/12(C))under CO_2 sequestration scheme. PR and AN acknowledge Council of Scientific and Industrial Research (CSIR), New Delhi, India for the award of CSIR fellowship.

References

1. Brydson J A 1999 In *Plastic Materials* 7th ed. Published by (Oxford: Butterworth-Heinemann)
2. Rao K N, Reddy B M, Abhishek B, Seo Y H, Jiang N and Park S E 2009 *Appl. Catal. B: Environ.* **91** 649
3. Li C, Miao C, Nie Y, Yue Y, Gu S, Yang W, Hua W, Gao Z and Chin 2010 *J. Catal.* **31** 993
4. Oliveira A C, Fierro J L G, Valentini A, Nobre P S S and Rangel M C 2003 *Catal. Today* **686** 49
5. Balasamya R J, Khurshida A, Al-Ali A A S, Atanda L A, Sagata K, Asamoto M, Yahiro H, Nomura K, Sano T, Takehira K and Al-Khattaf S S 2010 *Appl. Catal. A: Gen.* **390** 225
6. Sun A, Qin Z, Chen S and Wang J 2004 *J. Mol. Catal. A: Chem.* **210** 189
7. Lima C L, Campos O S, Oliveira A C, De Sousa F F, Filho J M, Neto P L, Correia A N, Sabadia G Q, Nogueira I M, Pinheiro G S and Oliveira A C 2011 *Appl. Catal. A: Gen.* **395** 53
8. Batista A H M, De Sousa F F, Honorato S B, Ayala A P, Filho J M, De Sousa F W, Pinheiro A N, De Araujo J C S, Nascimento R F, Valentini A and Oliveira A C 2010 *J. Mol.Catal. A: Chem.* **315** 86
9. Delgado J J, Chen X, Tessonnier J P, Schuster M E, Del Rio E, Schlogl R and Su D S 2010 *Catal. Today* **150** 49
10. Ansari M B and Park S E 2012 *Energy Environ. Sci.* **5** 9419

11. Sugino M, Shimada H, Turuda T, Miura H, Ikenaga N and Suzuki T 1995 *Appl. Catal. A: Gen.* **121** 125
12. Mimura N and Saito M 2000 *Catal. Today* **55** 173
13. Wang S and Zhu Z H 2004 *Energy Fuels* **18** 1126
14. Carja G, Nakamura R, Aida T and Niiyama H 2003 *J. Catal.* **218** 104
15. Badstube T, Papp H, Dziembaj R and Kustrowski P 2000 *Appl. Catal. A: Gen.* **204** 153
16. Li H, Yue Y, Miao C, Xie Z, Hua W and Gao Z 2007 *Catal. Comm.* **8** 1317
17. Li X H, Ying X W and Ke C 2005 *Catal. Lett.* **105** 223
18. Freire R M, Pinheiro A L, Oliveira A C, De Sousa F F, Ayala A P, Filho J M, Freire P T C and Oliveira A C 2009 *Appl. Catal. A: Gen.* **359** 165
19. Meima G R and Menon P G 2001 *Appl. Catal. A: Gen.* **212** 239
20. Burri D R, Choi K M, Sujandi D S H, Jiang N, Burri A and Park S E 2008 *Catal.Today* **131** 173
21. Burri D R, Choi K M, Han D S, Koo J B and Park S E 2006 *Catal. Today* **115** 242
22. Burri D R, Choi K M, Han S C, Burri A and Park S E 2007 *J. Mol. Catal. A: Chem.* **269** 58
23. Liao S J, Chen T, Miao C X, Yang W M, Xie Z K and Chen Q L 2008 *Catal. Commun.* **9** 1817
24. Sekine Y, Watanabe R, Matsukata M and Kikuchi E 2008 *Catal. Lett.* **125** 215
25. Jiang N, Han D S and Park S E 2009 *Catal. Today* **141** 344
26. Reddy B M, Lee S C, Han D S and Park S E 2009 *Appl. Catal. B: Environ.* **87** 230
27. Reddy B M, Jin H, Han D S and Park S E 2008 *Catal. Lett.* **124** 357
28. Ohishi Y, Kawabata T, Shishido T, Takaki K, Zhang Q, Wang Y and Takehira K 2005 *J. Mol. Catal. A: Chem.* **230** 49
29. Mathew T, Malwadkar S, Shivanand P, Sharanappa N, Sebastian C P, Satyanarayana C V V and Bokade V V 2003 *Cat. Lett.* **91** 217
30. Eduardo G and Alexander M 2004 *Appl. Catal. A: Gen.* **258** 99
31. Alexander M, Marıa E. Troconis, Eduardo G, Cesar Moran, Jorge Sanchez, Angel G and Jackeline Q 2006 *Appl. Catal A: Gen.* **310** 199
32. Xiao-Feng Guo, Joong-Ho Kim and Geon-Joong Kim 2011 *Catal. Today* **164** 336
33. Atanda L A, Balasamy R J, Khurshid A, Al-Ali A A S, Sagata K, Asamoto M, Yahiro H, Nomura K, Sanod T, Takehira K and Al-Khattaf S S 2011 *Appl. Catal A: Gen* **396** 107
34. Liu B S, Rui G, Chang R Z and Au C T 2008 *Appl. Catal. A: Gen.* **335** 88
35. Qiao Y, Miao C, Yue Y, Xie Z, Yang W, Hua W and Gao Z 2009 *Micro. Meso. Mater.* **119** 150
36. Carja G, Kameshima Y and Okada K 2008 *Micro. Meso. Mater.* **115** 541
37. Burri D R, Choi K M, Lee J H, Han D S and Park S E 2007 *Catal. Commun.* **8** 43
38. Zhao D, Feng J, Huo Q, Melosh N, Fredrickson G H, Chmelka B F and Stucky G D 1998 *Science* **279** 548
39. Kresge C T, Leonowicz M E, Roth W J, Vartuli J C and Beck J S 1992 *Nature* **359** 710
40. Jammaer J, Aerts A, Haen J D, Seob J W and Martens J A 2009 *J. Mater. Chem.* **19** 8290
41. Wang L, Mingming Zhang, Miao Zhang, Sha G and Liang C 2013 *Energy Fuels* **27** 2209
42. Jammaer J, van Erp T S, Aerts A, Kirschhock C E and Martens 2011 *J. Am. Chem. Soc.* **133** 13737
43. Wei D, Yao N and Haller G L 1999 *Stud. Surf. Sci. Catal.* **121** 239
44. Oliveira A C, Essayem N, Tuel A, Clacens J M and Taarit Y B 2008 *Stud. Surf. Sci. Catal.* **174** 1239
45. Wang J and Liu Q 2005 *Micro. Meso. Mater.* **83** 225
46. Gonzalez O, Perez H, Navarro P, Almeida L C, Pacheco J G and Montes M 2009 *Catal. Today* **148** 140
47. Wang C, Lim S, Du G, Loebicki C Z, Li N, Derrouiche S and Haller G L 2009 *J. Phys. Chem. C* **113** 14863
48. Taghavimoghaddam J, Knowles G P and Chaffee A L 2012 *J. Mol Cat. A: Chem.* **358** 79
49. Gregg S J and Sing K S W 1982 In *Adsorption Surface Area and Porosity* (London: Academic Press)
50. Tsoncheva T, Ivanova L, Minchev C and Froba M 2009 *J. Colloid Interface Sci.* **333** 277
51. Li J, Xu X, Hao Z and Zhao W 2008 *J. Por. Mat.* **15** 163
52. Szegedi A, Popova M and Minchev C 2009 *J. Mater. Sci.* **44** 6710
53. Li H, Wang S, Liang F and Li J 2006 *J. Mol. Catal. A: Gen.* **244** 33
54. Suvanto S and Pakkanen T A 2000 *J. Mol. Catal. A: Gen.* **164** 273
55. Szegedi A, PopovaM and Minchev C 2009 *J. Mater. Sci.* **44** 6710
56. Katsoulidis A P, Petrakis D E, Armatas G S, Trikalitis P N and Pomonis P J 2006 *Micropor. Mesopor. Mater.* **92** 71
57. Samuel P D, Anderson L P, Tiago P B, Antoninho V, Josue M F and Oliveira A C 2011 *J. Mol Cat. A: Chem.* **348** 1
58. Nogueira I M, Sabadia G Q, Moreira A A, Josue M and Oliveira A C 2011 *J. Mol. Cat. A: Chem.* **351** 81
59. Atanda L, Al-Yassir N and Al-Khattaf S 2011 *Chem. Eng. J.* **171** 1387
60. Ramudu P, Anand N V, Ramesh babu G, Mural Dhar G, Sai Prasad P S, David Raju B and RamaRao K S 2014 *Ind. J. Chem., Sec. A* **53A** 493
61. Zhao D, Huo Q, Feng J, Chmelka B F and Stucky G D 1998 *J. Am Chem. Soc.* **8 120** 6024